$(l^{N-1}\bar{\alpha}\bar{S}\bar{L}lSL\|\|l^N\alpha SL)$	Coefficient of fractional parentage as in Ref. 1 III.
$\bar{N}_\lambda, \bar{q}, \bar{q}_\lambda, \bar{\alpha}_\lambda, \bar{S}_\lambda, \bar{L}_\lambda$	Analogs of N_λ, q, q_λ, α_λ, S_λ, L_λ for spectator electrons.
$\tilde{\alpha}_\rho\tilde{S}_\rho\tilde{L}_\rho$	Intermediate quantum numbers in two-step parentage expansion (26).
$\epsilon=0, 1$	Index distinguishing alternative q that include a given $\bar{q}$.
$\bar{\psi}_{u\rho\sigma}$	Unsymmetrized product of spectator electron antisymmetric subshell wave functions coupled to wave functions of interacting electrons in subshells ρ and σ [Eqs. (25) and (27)].
Φ	Spin factor of $\bar{\psi}_{u\rho\sigma}$.
X	Orbital factor of $\bar{\psi}_{u\rho\sigma}$.
R^k	Slater integral as in Ref. 10.
$(l\|\|C^{(k)}\|\|l')$	Reduced matrix element as in Ref. 1 II or Ref. 9, FR, Chap. 14.
$(j_1j_2\cdots,\alpha\|\,j_1j_2\cdots,\alpha')^{(J)}$	Transformation matrix element, i.e., inner product of two different products of the same set of angular momentum eigenstates $(j_1j_2\cdots)$ whose momenta add up vectorially in different ways, distinguished by α and α', with the same resultant J. Replacement of α and α' by explicit description of vector couplings is a prerequisite of numerical evaluation.

ACKNOWLEDGMENTS

The author is indebted to numerous colleagues, particularly to Dr. F. Innes, Dr. G. Racah, and Dr. B. Wybourne, for discussions, advice, and literature references.

PHYSICAL REVIEW VOLUME 140, NUMBER 1A 4 OCTOBER 1965

Equilibrium Charge-State Populations of Carbon Ions from 2 to 10 MeV/amu in H_2, N_2, Ar, and Ni*

F. W. MARTIN
Department of Physics, Yale University, New Haven, Connecticut
(Received 16 April 1965)

Measurements of the equilibrium fractions of C^{6+}, C^{5+}, and C^{4+} ions as a function of ion energy have been made using a gas cell with differentially pumped exit slits and a magnet which spatially separates ions emerging from the slits in different charge states. The separated ion beams are intercepted with different thicknesses of foil and stopped in a junction counter, and charge-state populations are determined from the relative number of counts in each peak of the resulting pulse-height spectrum. Estimated errors are as small as ± 0.002 in the population and ± 0.05 MeV/amu in the energy. The rms charge of the ions is found to be a function of the material through which they are passing. The rms charge in gaseous N_2 and Ar is higher than in solids of neighboring atomic number at ion energies of 3 MeV/amu, but is the same in these gases and in the solids at 8 MeV/amu. At all energies measured, the charge in H_2 is anomalously high. The increased charge in solids is ascribed to a large electron-loss cross section at low energies, which shortens the time between collisions to the extent that the loss cross section is affected by excitation of the electron of the carbon ion. Estimates based on a crude model indicate that electron capture by the carbon ions takes place predominantly from the K shell of N_2 and the L shell of Ar. The anomalous charge in H_2 is apparently due to the absence of a shell from which capture is highly probable.

I. INTRODUCTION

ALTHOUGH considerable information has been obtained in recent years regarding the stopping of particles more massive than protons in the energy range between 2 and 10 MeV/amu,[1] less information is available concerning the charge of these ions as they are slowing down.[1,2] The fraction in each state of ionization has been measured for various ions in alumi-

* This work was supported by the U. S. Atomic Energy Commission. A preliminary report was given in Bull. Am. Phys. Soc. 11, 53 (1964). It was submitted together with Ref. 16 to the Faculty of Yale University in partial fulfillment of the requirements for the degree of Doctor of Philosophy.

[1] L. C. Northcliffe in *Annual Reviews of Nuclear Science* (Annual Reviews, Inc., Palo Alto, 1963), Vol. 13, p. 67.
[2] C. S. Zaidins, California Institute of Technology, 1962 (unpublished).

num[1] and in Zapon lacquer,[3] and the effective charge has been determined from stopping-power measurements for a variety of ions in oxygen and for fluorine ions in solids and gases.[4] At lower velocities, data are available for ions as heavy as Kr in various materials,[5,6] for oxygen and neon in gases,[7] for nitrogen in Formvar,[8] and for helium in gaseous and solid cadmium.[9] At lower velocities and for heavier particles, measurements have been made for halide ions in carbon,[10] fission fragments in gases,[11,12] and iodine ions in various solids.[13]

Measured charge-state populations are of immediate use in experimentation, for example in the determination of the rate of flow of particles from the current in an ion beam, and in the technology of acceleration and magnetic deflection of heavy-ion beams. They are also of importance in the comparison of presently available stopping-power measurements with theory since the stopping power in general depends on the mean-square charge and average charge of the ion[1] and the latter quantities may readily be obtained from the charge populations. For lack of better information it is usually assumed that the populations, and hence these charges, depend only on the velocity of the particle; however, it will be shown below, for the test case of the carbon ion, that while the velocity dependence accounts for most of the variation of the charge there is nevertheless a dependence on the nature of the stopping material.

Measurements of the charge state populations also provide one means of testing theoretical predictions for the relative rates of capture and loss of electrons by heavy ions, since the ratio of the populations of two charge states gives the ratio of the cross sections for transitions between these states. In general such theories contain many approximations due to the large number of electrons involved in a collision between a heavy ion and an atom of the stopping substance. However, in this experiment the carbon ion has a high probability of being stripped of all its electrons, and one of the stopping substances is hydrogen. In this relatively simple case comparison with accurate theoretical computations may be possible.

In the following, measurements of the fractions of carbon ions in the states of ionization C^{6+}, C^{5+}, and C^{4+} as a function of the velocity of the ion in H_2, N_2, Ar, and Ni are described. First the apparatus and general method of measurement are discussed. Next the procedures used in obtaining data, the precautions taken to ensure that unwanted effects were not present, and the steps taken in computing the results are given. After a description of the analysis of the data in nickel, the results are presented and are discussed empirically. Finally, the results are interpreted in the light of a crude theoretical estimate of the capture and loss cross sections as functions of ion velocity, and of the dependence of these cross sections on the state of excitation of the ion.

II. APPARATUS

A schematic plan view of the apparatus is shown in Fig. 1. A beam of carbon ions with 10 MeV of energy per amu of mass provided by the Yale Heavy Ion Accelerator (not shown) enters from the left. Shown at the left is a calibrated magnetic-analysis system, which serves to degrade the energy of the ions and to measure the degraded energy. In the center is a charge-exchange column containing gas at several millimeters of mercury pressure, in which the fraction of ions of each charge state in the beam reaches an equilibrium value characteristic of the gas and of the energy of the ions. At the right are the charge-analyzing magnet and counter, used to separate the ions of different charge states and to determine the number in each state.

A. Magnetic-Analysis System

The first magnet was used only as a bending magnet, aiming the ions at the $\frac{1}{4}$-in. slit, immediately in front of which were two foil wheels which in combination could provide many thicknesses of energy-degrading foil. The $\frac{1}{4}$-in. slit, the $\frac{3}{16}$-in. slit, and the second magnet formed a system which, when once calibrated, could be used to determine the energy of the degraded ions. The field strength at the edge of the vacuum chamber in the magnet was measured as a function of magnet current using a proton-resonance probe, and the effective radius of curvature of the ions in the magnet determined from the field strength required to deflect a beam of ions of known momentum. These ions were obtained from the first deflecting magnet which had previously been calibrated by field contour integration. The calibration was verified by measurements with an absolute magnetic spectrometer.[14] Relativistic formulas were necessary in computing $\mathcal{E}$, the kinetic energy of the ion in MeV divided by its rest mass in amu, from the momentum.

It was estimated that the systematic error in $\mathcal{E}$ was less than $\pm 0.5\%$ and that the spread of energies which

[3] H. H. Heckman, E. L. Hubbard, and W. G. Simon, Phys. Rev. **120**, 1240 (1963).
[4] P. G. Roll and F. E. Steigert, Phys. Rev. **120**, 470 (1960).
[5] V. S. Nikolaev, I. S. Dimitriev, L. N. Fateev, and Ya. A. Teplova, Zh. Eksperim. i Teor. Fiz. **33**, 1325 (1957) [English transl.: Soviet Phys.—JETP **6**, 1019 (1958)].
[6] V. S. Nikolaev, I. S. Dimitriev, L. N. Fateeva, and Ya. A. Teplova, Zh. Eksperim. i Teor. Fiz. **39**, 905 (1960) [English transl.: Soviet Phys.—JETP **12**, 627 (1961)].
[7] E. L. Hubbard and E. J. Lauer, Phys. Rev. **98**, 1814 (1955).
[8] H. L. Reynolds, L. D. Wyly, and A. Zucker, Phys. Rev. **98**, 474 (1955).
[9] W. Meckbach and S. K. Allison, Phys. Rev. **132**, 294 (1963).
[10] E. Almquist, C. Broude, M. A. Clark, J. A. Kuehner, and A. E. Litherland, Can. J. Phys. **40**, 954 (1962).
[11] N. O. Lassen, Kgl. Danske Videnskab. Selskab, Mat. Fys. Medd. **26**, No. 5 (1951).
[12] N. O. Lassen, Kgl. Danske Videnskab. Selskab, Mat. Fys. Medd. **26**, No. 12 (1951).
[13] C. D. Moak and M. D. Brown, Phys. Rev. Letters **11**, 284 (1963).
[14] The spectrometer is described in L. C. Northcliffe, Phys. Rev. **120**, 1744 (1960).

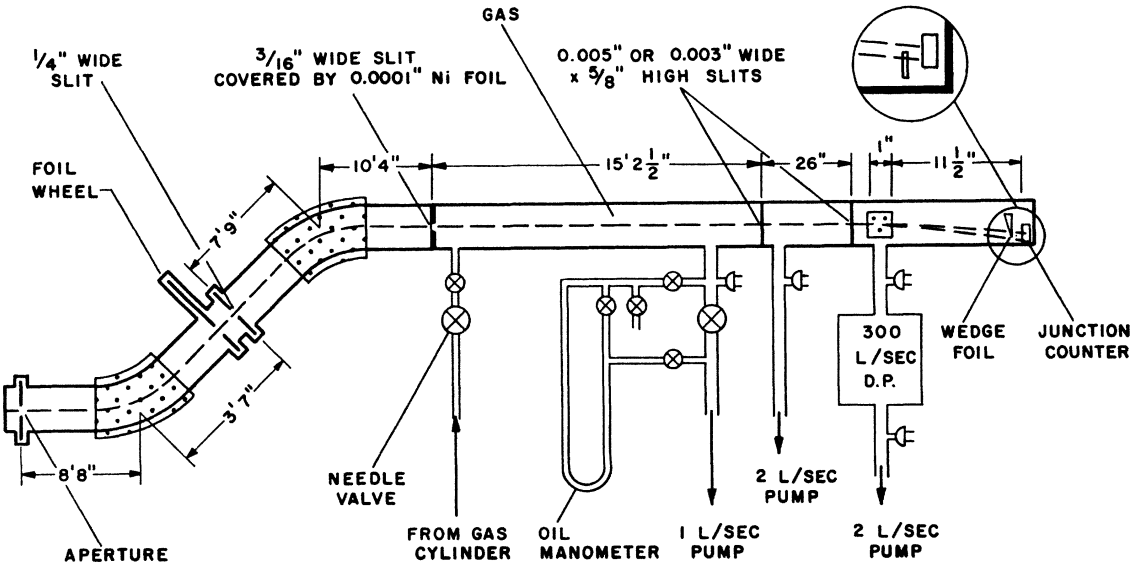

FIG. 1. Schematic plan view of the apparatus (not to scale). Accelerated carbon ions are slowed to velocities of 1.9×10^9 to 4.4×10^9 cm/sec in one of the foils located in the foil wheel, and, after their momentum is defined by the second magnet, they traverse of the order of 1 mg/cm² of gas in the charge-exchange column. Upon emerging from the gas without passing through any foil the ions are separated into beams according to their charge as they pass through the third magnet, and the number in each beam is determined using a single junction counter.

could pass through the second magnet was about $\pm0.6\%$. Further reduction of either the systematic or random errors was not necessary, considering the large uncertainties in the populations and their slow change with energy.

B. Charge-Exchange Column

The $\frac{3}{16}$-in. slit at the entrance to the charge-exchange column was also a holder for a 0.0001-in. nickel foil which retained the gas inside the column. In the foil the beam of C^{5+} ions was converted to a mixture of C^{6+} and C^{5+}, and this equilibrium beam emerged into the gas. Equilibrium seems to be assured since the areal density of the foil was 2.28 mg/cm², compared with the 0.2 mg/cm² found[3] necessary to ensure equilibrium for 10 MeV/amu argon ions in Zapon.

The gas was maintained at a pressure of several millimeters of mercury in dynamic equilibrium between a needle valve inlet and a differential pumping system. To prevent contamination by air, the gas between the needle valve and the pressure-reducing valve was kept above atmospheric pressure. The constrictions of the differential pumping system were two slits which also collimated the ions before they entered the charge-analyzing magnet. Behind the first slit a mechanical forepump was connected, and behind the second a diffusion pump. At the maximum operating pressure used in the charge-exchange column, the maximum pressure at the charge-analyzing magnet was 40μ Hg.

Pressure in the charge-exchange column was measured using an oil manometer filled with pump oil of low vapor pressure and measured density. Reference pressure was supplied by a mechanical forepump, which also served to evacuate the charge-exchange column when the gas was changed. Pressures at other points in the system were measured with temperature-compensated thermocouple gauges. The ultimate vacuum in the charge-exchange column was 0.010 mm Hg. Using this measurement of pressure, a value[15] of 0.12 liter/sec for the conductance of the first slit, and the assumption that the pressure behind the slit was zero, an upper limit of 0.0012 mm liter/sec can be estimated for the flow through the first slit. If this flow is attributed to leaks, it could not contaminate the gas more than 0.25%, since the normal flow through the slit was typically 0.4 mm liter/sec. The purity of the gases themselves was stated to be 99.9% or better by their manufacturers.

C. Charge-Analyzing Magnet and Counter

After being collimated by the differential pumping apertures, the ions passed between the poles of an electromagnet, which deflected the C^{6+} ions more than the C^{5+} ions, causing a horizontal separation of the two beams of about 2.3 mm magnitude in the region of the counter. To minimize errors due to change of charge of the ions while they were being deflected, the region of magnetic field was made short. Outside the magnetic field charge change did not matter, since no change in direction of the ions resulted and therefore the number of ions in each beam did not change.

The charge-analyzing magnet had pole pieces 1 in.

[15] See S. Dushman, *Scientific Foundations of Vacuum Technique* (John Wiley & Sons, Inc., New York, 1949), p. 92, Eq. (6a) with $A=0.5$ in.$\times0.003$ in.

by 1 in. in cross section and a gap of $\frac{3}{8}$ in. The field strength at the center of the gap was determined as a function of the magnet current using a rotating coil fluxmeter, and the system was calibrated using the alpha particles from a Po^{210} source ($\mathcal{E}=1.3$ MeV/amu), placed in front of the first differential pumping aperture.

Ions were detected by a junction counter, commercially fabricated by diffusion of phosphorus into 5000 ohm cm p-type silicon, placed $\frac{1}{2}$ in. behind a $\frac{1}{8}$-in.-wide horizontal slit, narrower than the sensitive region of the detector. Multiple scattering in the charge-exchange gas was assumed to cause enough angular divergence in the beams to make their vertical spread before passing through the horizontal slit comparable to the $\frac{1}{2}$-in. height of the differential pumping apertures. The pulses from the counter passed through a charge-sensitive preamplifier, a long coaxial cable, an attenuator, and a double-delay-line-clipped linear amplifier, and were sorted by an RIDL 400-channel analyzer. The linearity of the entire system was checked before and after each run using pulses from a Victoreen calibrated pulse generator capacitatively coupled to the preamp input.

Discrimination of the two beams striking the counter was usually achieved by intercepting the beams with different thicknesses of aluminum foil, so that they lost different amounts of energy and appeared as separate peaks in the pulse-height spectrum. The foils were made either by laminating commercial uniform foil in staircase fashion or by abrading and polishing a single foil to the desired taper.

III. THE EXPERIMENT

A. Collection of Data

Most of the data were taken using laminated foils with several steps each 2.3 mm long, so that for the normal deflection of 14 mm for the charge-6 ions, each charge state would fall in the center of a step. A typical pulse-height spectrum obtained with this arrangement is shown in Fig. 2(a). The lack of separation of the peaks in this spectrum was attributed to a low-energy tail for each peak, probably caused by slit-edge scattering. Subsequent runs were made with the thinner foil in the path of the charge-5 beam, so that the less populous 5's would appear at higher pulse heights than the 6's, in a region where there was no low-energy tail from the charge-6 peak. An example of the improved separation given by this procedure is shown in Fig. 2(b). At low energies the charge-4 ions became detectable, and in this case the magnetic deflection was usually increased to such an extent that the charge-6 ions did not enter the sensitive region of the counter. The beam current could then be increased and the few charge-4 ions counted more rapidly.

When the step foils were used, it was necessary to ensure that each beam passed only through a single step. To meet this condition the position of the steps was located using the ion beams. While energy was kept constant the counting rate of ions penetrating a given step was recorded as a function of magnetic deflection. The positions of the two edges of a step were given by the deflections at which the counting rate appropriate to charge-6 ions appeared and disappeared. This method was also used to determine the spatial width of the beam. The value obtained from a scan with 8 points in the transition region was 0.4 ± 0.1 mm full width at half maximum (fwhm) compared to a trapezoidal distribution of 0.2 ± 0.1 mm fwhm expected with the nominally 0.005-in. collimating slits which were in place.

When the data were analyzed the magnetic deflection for each spectrum was computed and compared to the

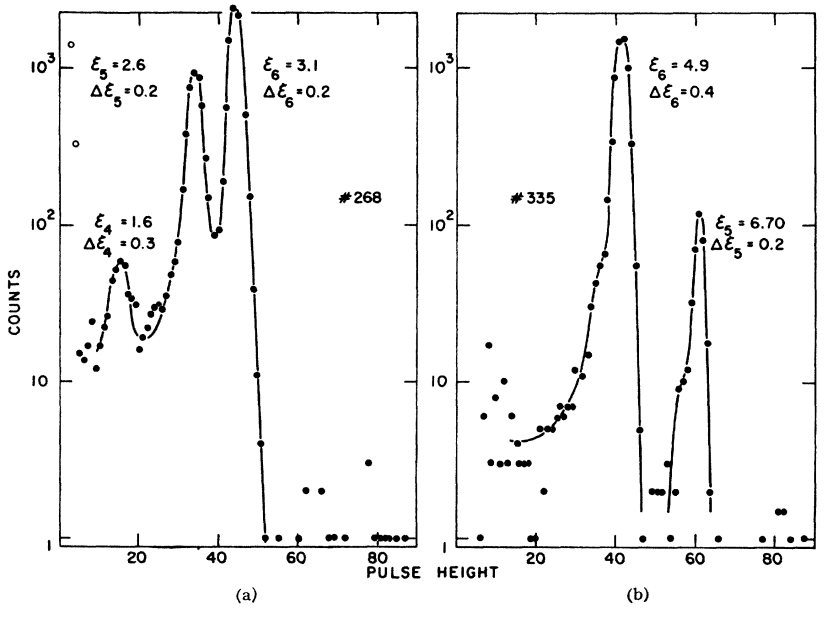

FIG. 2. Typical pulse-height spectra in the junction counter with uniform foils of differing thickness intercepting each beam. At the left is a spectrum in which the less intense beams intercepted the thicker foils; at the right is one in which the more intense beam intercepts the thicker foil.

transition deflection. Spectra for which the center of a beam came within 0.3 mm of a transition were discarded, as were spectra for which a beam fell partly off the counter. As a further check, the energies determined from the pulse height of each peak were plotted versus the energy in the analyzing magnet, and the experimental points compared to curves calculated from range-energy data for carbon ions in aluminum using the known thicknesses of the foils. Inconsistent points were investigated and satisfactory agreement obtained.

B. Nonequilibrium Effects

To demonstrate that the carbon ions had traveled far enough in the gas to reach equilibrium, the populations of the charge states of carbon ions in hydrogen were measured as a function of gas pressure at 6.9 MeV/amu. The fraction ϕ_5 of ions with 5 electrons removed is shown as a function of pressure, or alternatively, areal density of gas, in Fig. 3. It is apparent that ϕ_5 has approached its equilibrium value to within the errors at the typical pressure of 3 mm Hg used in the experiment. Since the areal density required to reach

TABLE I. Electron capture and loss cross sections for carbon ions in hydrogen gas at 6.9 MeV/amu.

Values used in Eq. (1)		
$\phi_5(0)$	$\sigma_{65}/(\sigma_{56}+\sigma_{65})$	$\sigma_{56}+\sigma_{65}$
0.030	0.003	5.9×10^{-20} cm^2
Loss cross section		
	$\sigma_{56}/\pi a_0^2=6.5\times10^{-4}$	
Capture cross section (see Sec. VI of text)		
	$\sigma_{65}/\pi a_0^2=2\times10^{-6}$	

equilibrium decreases as the energy of the ions decreases,[7] equilibrium is assured below 7 MeV/amu. If the electron-capture and loss cross sections of the ion are not markedly smaller in nitrogen and argon, equilibrium also occurs in these gases.

Figure 3 is also of interest in another respect. When the gas is evacuated from the charge-exchange cell (zero pressure in the figure), ϕ_5 assumes the equilibrium population for carbon ions in the nickel entrance foil. Since this value is higher than the value of ϕ_5 at large pressures the figure shows that the average charge of the carbon ion is lower in nickel than in hydrogen gas.

An approximate value of the cross sections for electron capture and loss from the ion may also be derived from these measurements. If we assume that ϕ_4 is negligible, and that the electron-capture cross section σ_{54} of the charge-5 carbon ion is also negligible, the equations[1] for the rates of change of ϕ_6 and ϕ_5 in the gas have the solution

$$\phi_5(s)=\sigma_{65}/(\sigma_{56}+\sigma_{65}) +[\phi_5(0)-\sigma_{65}/(\sigma_{56}+\sigma_{65})]e^{-(\sigma_{65}+\sigma_{56})Ns}, \quad (1)$$

where s is the distance traveled and N the number of gas atoms/cm^3. The characteristic distance of this exponential, which can be determined from the data,

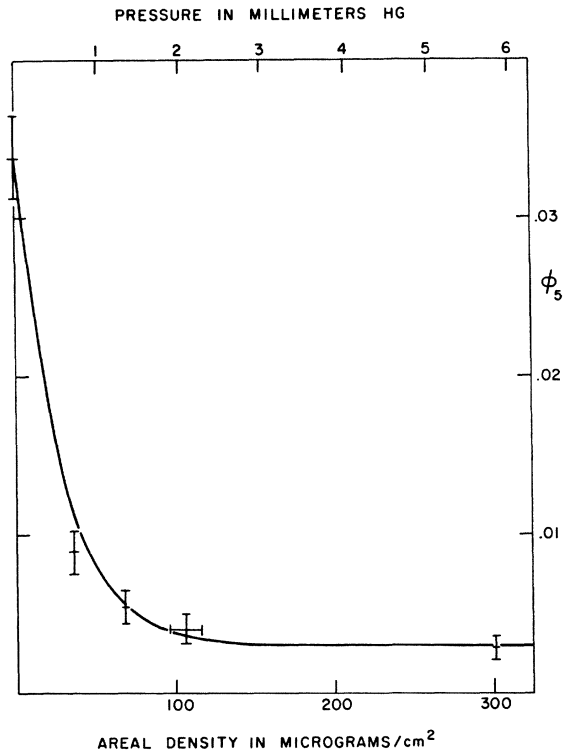

FIG. 3. The fraction of 6.9-MeV/amu carbon ions with 5 electrons removed, as a function of hydrogen gas thickness which they have traversed, showing the approach of the fraction to equilibrium. The ions enter the gas from a nickel foil in which the equilibrium fraction is seen to be higher than in hydrogen.

gives a value for the sum of the two cross sections, and the value which it approaches at large values of Ns gives the ratio of σ_{65} to the sum. The individual cross sections can be computed readily from these quantities. The results of this procedure are given in Table I, in which the parameters used in Eq. (1) to compute the smooth curve of Fig. 3 are given, as well as the values of the cross sections. The capture cross section has a magnitude of about 100 b.

In addition to nonequilibrium effects, a second possible source of variation in the equilibrium populations was investigated. It has been found that the equilibrium charge of fission fragments in a given gas varies with the gas pressure.[12] As will be seen presently, the process responsible for this variation is not expected with carbon ions at the velocities and gas pressures of this experiment. No variation of the equilibrium populations with pressure was found in the final data, although the pressure was purposely varied between 2 and 5.5 mm Hg in the measurements with nitrogen gas.

C. Reduction of Data

The energy of the ions at the charge-analyzing magnet differed from the energy determined by the magnetic analysis system because of energy loss in the nickel foil and in the charge-exchange gas itself. The loss in the gas varied with the energy of the ions, with gas pressure,

TABLE II. Typical uncertainties in the energy-loss correction, computed for a gas thickness of 8 mg/cm² aluminum equivalent.

Source	Amount	Uncertainty (mg/cm²)
Foil thickness	2.28±0.05 mg/cm²	±0.12
Gas pressure	5±0.1 cm oil	±0.16
Gas temperature	300±3°K	±0.08
		Sum = ±0.36
Maximum slope of range curve for proton in aluminum	$=0.1\frac{\text{MeV/amu}}{\text{mg/cm}^2}$	
Uncertainty in $\mathcal{E}$	= ±0.04 MeV/amu	

and with the molecular weight of the gas and was normally between 1 and 5 times as great as the loss in the nickel. The largest loss, suffered at low energy and high gas pressure, was 1.34 MeV/amu. The energy losses were computed using range-energy data for carbon ions in gases[16] and in nickel.[17]

Typical uncertainties in the energy loss correction are shown in Table II. Combined nickel and gas thicknesses up to 24 mg/cm² Al equivalent were used; hence uncertainties as large as ±0.12 MeV/amu could occur. At large energies the uncertainty actually is smaller than estimated, because the slope of range-energy curve decreases with $\mathcal{E}$. In the middle range of energies of the experiment, the uncertainty in the correction becomes smaller than the 0.5% random error in $\mathcal{E}$ itself. The random error arising from both $\mathcal{E}$ and its correction is probably about 0.05 MeV/amu at any value of $\mathcal{E}$.

The fraction ϕ_i of ions with i electrons removed was calculated from the number of counts in the corresponding peak of the pulse height spectrum. When only one exposure was taken, the fractions were calculated using the relation

$$\phi_i = N_i / \sum_j N_j, \tag{2}$$

where N_i is the number of counts in the ith peak and $\sum_j N_j$ is the total number of counts. In cases where two exposures were taken, the first giving values for N_6 and N_5, and the second values for N_5' and N_4', the fractions were computed from the equations

$$\phi_4\left[1+(N_5'/N_4')\left(1+\frac{N_6}{N_5}\right)\right]=1;$$
$$\phi_5=(N_5'/N_4')\phi_4; \quad \phi_6=(N_6/N_5)\phi_5. \tag{3}$$

Before satisfactory separation of the peaks was attained, the following procedure was used to determine values of N_i and their uncertainties. The peaks were assumed to have a low-energy tail, and the peaks at lower pulse heights were assumed to be superimposed on the large tail of the uppermost peak. The tails were disregarded on the grounds that they contained equal percentages of the counts in their respective peaks, and only counts under the peaks and above any tail were summed. Because of the uncertain origin of the tails, a background error estimate, given by the product of half the background counting rate per channel (as determined at small pulse heights) and the width at the base of the peak in question, was assigned to each peak sum. In addition, in those cases where the valley between peaks did not approach a value near the counting rate at low pulse height, a separation error equal to the counting rate per channel in the valley was assigned to the sums for the peaks on either side. These two error estimates were combined with the statistical standard deviation to give an estimate of the total error in the number of counts in a peak.

When satisfactory separation between the peaks was attained, only the statistical uncertainties were significant.

IV. A PREVIOUS MEASUREMENT FOR NICKEL

In previously reported measurements[16] the ion beams emerging from the nickel window of a gas cell were deflected by a uniform magnetic field and recorded on a strip of 16-mm motion picture film. The various charge states of the ions appeared as lines on the developed film, and the darkness of a line indicated qualitatively the population of the corresponding charge state.

To determine the number of ions which had struck the film, the optical density of the lines was measured with a recording densitometer, producing on a chart recorder a trace of optical density as a function of magnetic deflection of the ions. It is plausible to assume that the optical density above fog at a point on the film corresponds to the number of ions striking per unit area at that point.[18] On this assumption the area of the chart recording for each line which lay above the fog density was measured with a planimeter, and the values of the area were used in Eq. (2) to determine the corresponding charge state populations. Lines with peak optical densities greater than 1.5 were excluded from the data except for the two points above 8 MeV/amu. For these two points the values given for ϕ_6 and ϕ_5 are probably too small and too large, respectively, because of photographic saturation of the charge-6 line.

TABLE III. Typical uncertainties in densitometer measurements of area.

Energy of ions (MeV/amu)	2.45	2.45	2.45
Charge state of ion (electronic charges)	+6	+5	+4
Linearity of densitometer (percent)	3	3	3
Base line (percent)	0.7	2	10
Planimeter reproducibility (percent)	1.8	3.7	37.5
Net estimate (percent)	5	7	42

[16] F. W. Martin and L. C. Northcliffe, Phys. Rev. **128**, 1166 (1962).
[17] P. G. Roll and F. E. Steigert, Nucl. Phys. **17**, 54 (1960).
[18] See Ref. 1, footnote 9, and Ref. 16, footnote 10.

The estimated uncertainties of the populations for a representative case are shown in Table III, together with the sources and estimated magnitudes of their component uncertainties. The fractional error in area was taken to be the fractional error in ϕ_i.

For comparison with results obtained as above, data were taken when the charge-exchange column was evacuated to forepump pressure (shown as solid circles in Fig. 7). In this case the populations were those established in the nickel entrance foil to the charge-exchange column. It is seen that the measurements with two types of apparatus agree within the experimental errors.

V. RESULTS AND SYSTEMATIC TENDENCIES

In Figs. 4–7 the equilibrium fractions ϕ_i of carbon ions are plotted as a function of their energy per unit mass. The solid curves are drawn freehand. In all these figures the error bars for most of the values of ϕ_6 have been omitted because of their smallness. In the data for nickel, the remaining error bars are shown for typical points. In the data for gases error bars have been shown for all values of ϕ_4 but with one exception for only the more accurate values of ϕ_5. The single large error bar is included for each gas to show the typical uncertainty of the ϕ_5 points without error bars. These measurements form a family taken before the best separation of peaks in the pulse-height spectra was obtained. Values taken

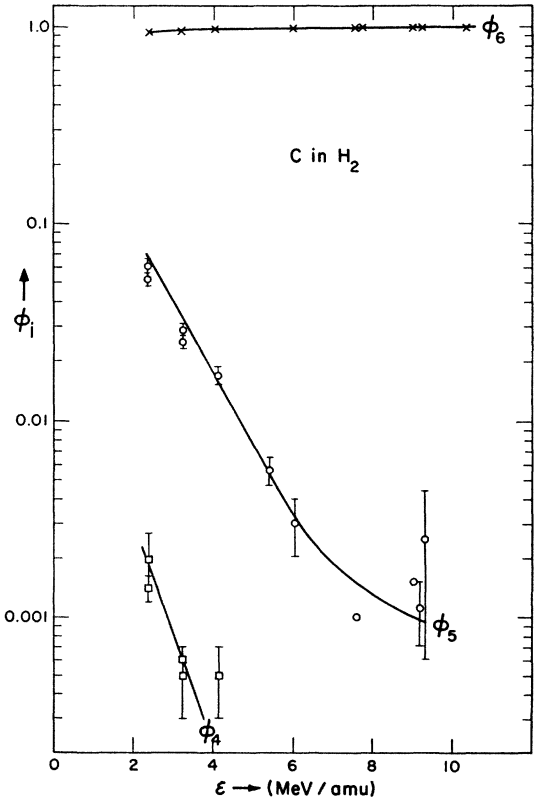

FIG. 4. Equilibrium charge-state populations for carbon ions in hydrogen. The equilibrium fraction ϕ_i of ions with i electrons missing is plotted versus the energy per unit mass of the ions.

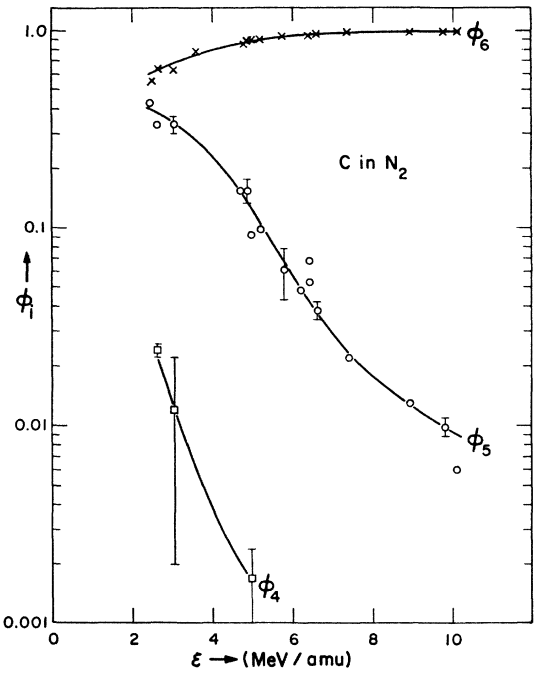

FIG. 5. Equilibrium charge-state populations for carbon ions in nitrogen.

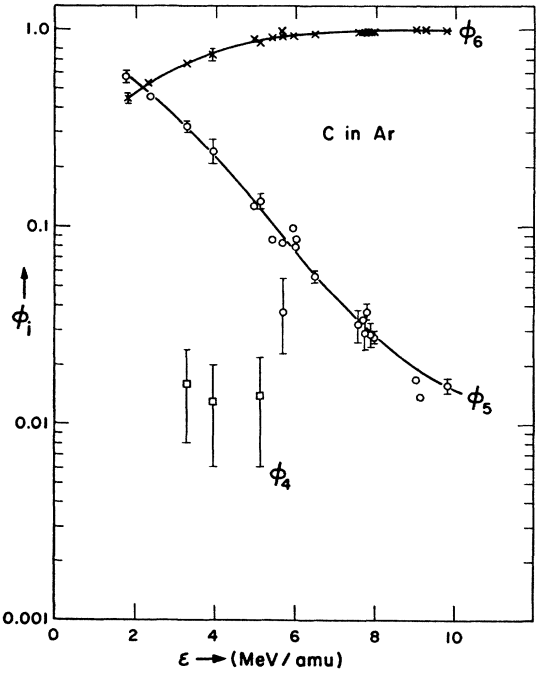

FIG. 6. Equilibrium charge-state populations for carbon ions in argon.

TABLE IV. Charge-state populations of C^{12} ions in hydrogen, nitrogen, argon, and nickel. Values of the equilibrium fractions ϕ_i taken from the freehand curves of the figures are listed. See Ref. 19 for a tabulation of the measured values and estimated errors for all points shown in the figures.

$\mathcal{E}$ (MeV/amu)		10	9	8	7	6	5	4	3	2
Stopping substance	ϕ_i	Values of ϕ_i for the above values of $\mathcal{E}$								
H_2	ϕ_6		0.9989	0.9983	0.997	0.996	0.992	0.983	0.962	
H_2	ϕ_5		0.0011	0.0017	0.0026	0.004	0.008	0.017	0.037	
H_2	ϕ_4								0.0008	
N_2	ϕ_6	0.991	0.988	0.982	0.970	0.942	0.87	0.76	0.65	
N_2	ϕ_5	0.009	0.012	0.018	0.030	0.058	0.13	0.24	0.34	
N_2	ϕ_4						0.0017	0.004	0.013	
Ar	ϕ_6	0.985	0.980	0.972	0.956	0.92	0.87	0.76	0.62	
Ar	ϕ_5	0.015	0.020	0.028	0.044	0.076	0.13	0.23	0.36	
Ar	ϕ_4							0.01	0.02	
Ni	ϕ_6	0.986	0.982	0.975	0.964	0.944	0.91	0.85	0.74	0.58
Ni	ϕ_5	0.014	0.018	0.025	0.036	0.056	0.09	0.15	0.24	0.37
Ni	ϕ_4								0.02	0.05

from the freehand curves of the figures are listed in Table IV.[19]

The data show that in a velocity region where the carbon ion rarely carries more than one electron, the charge of the ion is a function of the material through which it passes. This can be seen by comparison of Figs. 4 to 7, in which values of ϕ_5 at a given velocity are much lower for hydrogen than for any other material, and the values of ϕ_5 for nitrogen, argon, and nickel often differ by more than the estimated errors. For example at $\mathcal{E}=3$ MeV/amu the value of ϕ_5 for nickel is significantly lower than those for the gases, although at $\mathcal{E}=10$ MeV/amu its value is the same as that for either gas within the appreciable uncertainties. In addition, while the values of ϕ_5 for the two gases are not significantly different at $\mathcal{E}=3$ MeV/amu, the value for nitrogen is lower than that for argon at $\mathcal{E}=10$ MeV/amu.

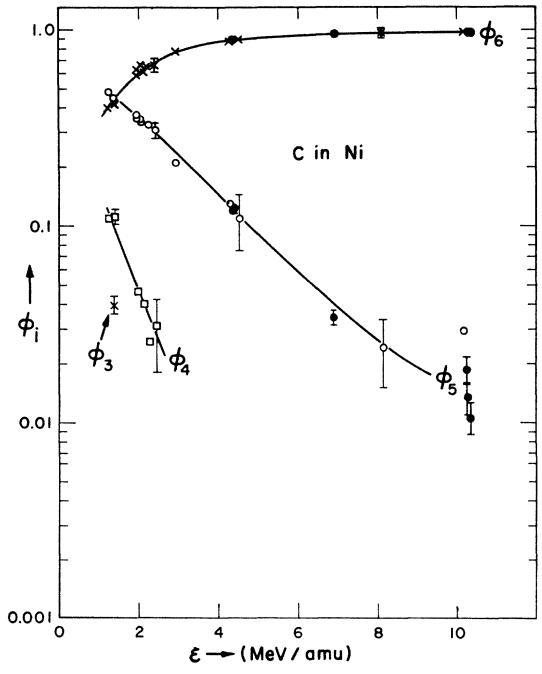

FIG. 7. Equilibrium charge-state populations for carbon ions in nickel.

As a means of summarizing the variation of the charge of the ion with stopping material and velocity, the root-mean-square (rms) charge is plotted as a function of the Z of the material at $\mathcal{E}=3$ and 8 MeV/amu in Fig. 8. Additional data for aluminum[1] and for the organic material Zapon[3] are included. It is apparent that the charge in hydrogen is anomalously high at both energies. For the stopping materials of higher Z, the charge at $\mathcal{E}=3$ MeV/amu is higher in solids than in gases, while at $\mathcal{E}=$ MeV/amu it is the same in solids and gases within the experimental errors.

VI. DISCUSSION

If the probability of multiple electron capture or loss is negligible the populations of the charge states of C^{6+} and C^{5+} ions are related to the cross section σ_{65} for capture and σ_{56} for loss of a single electron by the equation

$$\phi_6/\phi_5=\sigma_{56}/\sigma_{65}. \quad (4)$$

To provide a means for the interpretation of the present data, a crude method for the calculation of these cross sections will be described below. It will be applied to the case of carbon ions in gases in an attempt to explain the anomalous results in hydrogen. The situation which leads to an increase of the charge in solids will then be discussed.

For the purposes of this discussion, an atom will be regarded as having its electrons in independent shells, each characterized by ionization potential I_p, principal

[19] Complete original data, consisting of values of $\mathcal{E}$, ϕ_i, estimated error in ϕ_i, and gas pressure for each point shown in the figures, are given in the author's Ph.D. thesis. These data have also been deposited as Document No. 8474 with the ADI Auxiliary Publications Project, Photoduplication Service, Library of Congress, Washington 25, D. C. A copy may be secured by citing the document number and by remitting $1.25 for photoprints, or $1.25 for 35-mm microfilm. Advance payment is required. Make checks or money orders payable to: Chief, Photoduplication Service, Library of Congress.

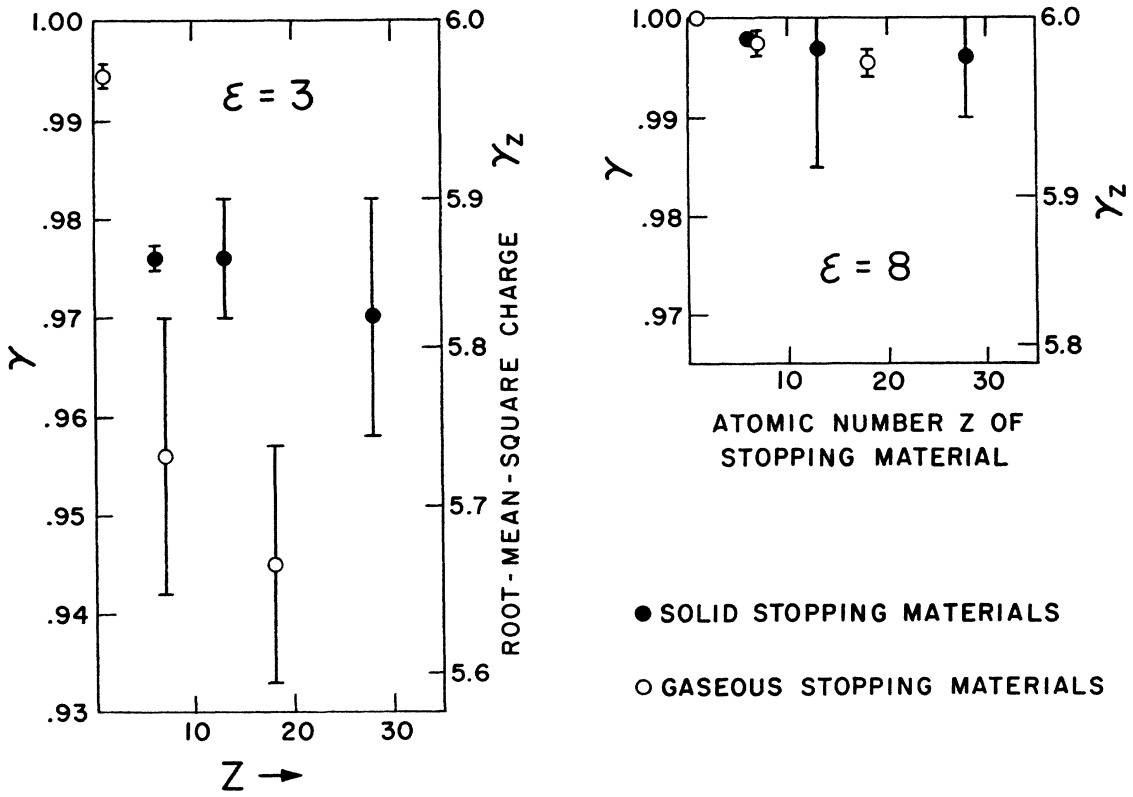

FIG. 8. The rms charge of carbon ions at two energies in solids and gases, as a function of the atomic number of the stopping material. If hydrogen gas is excepted the charge is higher in solids than in gases at the lower energy. The parameter γ is the ratio of the rms charge to the nuclear charge of the ions.

quantum number n, and radius a_p. The value of a_p is given by the formula

$$a_p = a_0 n^2/(Z-k), \tag{5}$$

where a_0 is the radius of the first Bohr orbit of hydrogen, Z is the atomic number of the atom, and k is the amount by which the nuclear charge is screened by inner shells of electrons.

A. Loss Cross Section

The cross section for loss of one electron from a C^{5+} ion may be estimated by extending the range of applicability of the free collision approximation.[20] In this approximation, only those encounters between atoms and ions are considered in which the center of a gas atom has an impact parameter x smaller than the orbital radius a_q of the electron in the ion. In encounters with larger impact parameters, the effects of the electrons and nucleus of the atom upon the electron of the ion are assumed to cancel. Upon further assumption that the electrons and nucleus of the atom act as independent point charges during the closer collisions, the expression

$$\sigma_{56}/\pi a_0^2 = 2(mv_0^2/I_q)(v_0/v)^2(Z^2+Z) \tag{6}$$

is obtained, in which I_q is the ionization potential of the electron of the ion, v is the velocity of the ion, and $v_0 = e^2/\hbar$. For the conditions listed in Table I, Eq. (6) gives $\sigma_{56}/\pi a_0^2 = 7.7\times10^{-4}$.

The above formula was derived on the assumption that $\kappa = 2Zv_0/v < 1$. Table V lists the values of κ in the present experiment, and it is seen that $\kappa > 1$ for the heavier gases. However, if $\kappa > 1$, collisions with $x < i_q = \kappa a_q$ are still free,[21] provided that the impact parameter

TABLE V. Parameters in the collisions of various projectiles with the electron of a C^{5+} ion.

Projectile	Parameter	Value at 3 MeV/amu	Value at 10 MeV/amu
Proton	κ	0.18	0.10
	i_q/a_0	0.028	0.015
Nitrogen nucleus	κ	1.3	0.70
	i_q/a_0	0.21	0.11
Argon nucleus	κ	3.3	1.8
	i_q/a_0	0.53	0.30
Electron	κ	0.18	0.10
	i_q/a_0	0.014	0.0076
Any of the above	d_q/a_0	0.61	1.1
	a_q/a_0	0.16	0.16

[20] N. Bohr, Kgl. Danske Videnskab. Selskab, Mat. Fys. Medd. **18**, No. 8 (1948), p. 107.

[21] See Ref. 20, p. 82. In this work the duration of a collision with impact parameter x is taken to be v/x rather than $2\pi v/x$, causing $\hbar$ rather than $\hbar$ to appear in the expression for the adiabatic impact parameter.

i_q at which the ionization energy I_q is transferred to a free electron is smaller than the adiabatic impact parameter $d_q=h\nu/I_q$. Table V shows this condition to be satisfied, so that the free-collision approximation may still be used as a basis for an estimate. However, in heavy gases the free collisions for which $a_q<x<i_q$ will have little ionizing effect, because of the assumed cancellation of forces when $x>a_q$, and the loss cross section in these gases should be smaller than that computed for free collisions.

In addition the inner electrons of heavy atoms will remain bound to the nucleus and will not act as independent scattering centers for the electron of the ion even in close collisions.[20] Instead they will shield the nucleus, reducing both the Z^2 and Z term in Eq. (6). This effect, which has been shown to be relevant even in hydrogen,[22] will also result in cross sections smaller than those computed for free collisions.

Values computed using Eq. (6) are shown in Table VII.

B. Capture Cross Section

The cross section for capture of an electron by a C^{6+} ion may be computed using the Born approximation. For the amplitude of the qth eigenfunction of the electron about the nucleus of the ion after the collision this yields,[23] using the present notation

$$b_{pq}=-\frac{i}{\hbar}\int_{-\infty}^{\infty}dt\, e^{-(I_q-I_p-\frac{1}{2}mv^2)it/\hbar}V_{qp}(t,x), \qquad (7)$$

in which t denotes time, and $V_{qp}(t,x)$ is an integral containing the wave functions of the electron about the ion and the atom, the potential of the atom, and a sinusoid. Equation (7) may be used to elucidate the qualitative features of the collision and to provide an estimate of the cross section.

The integral $V_{qp}(t,x)$ contains an overlap of the wave functions of the ion and the atom and will be appreciably different from zero only when the two are close together. In order for b_{pq} to be large, $V_{qp}(t,x)$ must rise and fall in a time comparable to the period of the exponential. If the time of interaction is too long, the rapidly varying exponential will cause b_{pq} to be small. The time may be measured as $2\pi x/v$ and the collisions will be adiabatic if

$$|2\pi x/v|>|\hbar/(I_q-I_p-\tfrac{1}{2}mv^2)|, \qquad (8)$$

or for x greater than

$$c_p=\frac{\hbar v}{|I_q-I_p-\frac{1}{2}mv^2|}. \qquad (9)$$

Equation (9) differs from that for the adiabatic impact parameter $\hbar v/I_p$ for ionization of the electron of the atom, but is similar in its comparison of the time of interaction to the quantum-mechanical period $h/\Delta E$. In the present case the energy of the electron before the collision is $(-I_p)$, while afterwards it is $\frac{1}{2}mv^2+(-I_q)$, because the electron has kinetic energy in the frame of the reference fixed at the atom; the difference is $\Delta E=I_q-I_p-\frac{1}{2}mv^2$.

In addition to yielding an area πc_p^2 outside of which the collision becomes adiabatic, Eq. (7) can be used to estimate the probability of transition for collisions with impact parameters smaller than c_p. In these encounters, the time a_p/v over which $V_{qp}(t,x)$ is of appreciable magnitude usually exceeds the period c_p/v of the exponential in Eq. (7). To estimate the value of b_{pq}, the integration may be taken over a time $\Delta t=c_p/v$ for which $V_{qp}(t,x)$ is large. The maximum value of $V_{qp}(t,x)$ at $t=0$ may be estimated by writing

$$V(r)=(Z-k)e^2/r \qquad (10)$$

for the potential in the atom seen by the electron and by assuming the wave functions are constant inside radii a_p, a_q (and zero outside), with the result that

$$V_{qp}(0,x)=(Z-k)e^2/a_{pq}, \qquad (11)$$

where

$$a_{pq}=\tfrac{2}{3}a_l(a_l/a_s)^{1/2}, \qquad (12)$$

in which a_l is the larger of a_p, a_q and a_s is the smaller. Multiplication of Δt and $V_{qp}(0,x)$ then gives a value of b_{pq}, from which the transition probability θ may immediately be found:

$$\theta=|b_{pq}|^2=[(Z-k)(v_0/v)(c_p/a_{pq})]^2. \qquad (13)$$

Table VI shows the computation of capture cross sections using Eq. (9) to evaluate $(c_p/a_0)^2$ and Eq. (13) to compute θ. The area inside of which nonadiabatic transitions can occur does not vary widely: It decreases as the binding energy of the electron in the atom increases and is markedly small only for the K electrons of argon. However, the transition probabilities vary widely, and when $a_p\approx a_q$ they even have computed values larger than unity. In such a case the original Eq. (7) fails because it is assumed in its derivation that the wave function of the electron in the atom does not change during the collision; obviously this is not true if the probability of capture of the electron is large. One expects[24] oscillatory behavior in which an electron in a state ultimately leading to capture makes a transition back to a state of the atom, and then again to "capture," and so on.

The computations for shells in which θ is small are more likely to have some significance as estimates, and the contribution of these shells to the cross section is nearly two orders of magnitude smaller than that of the shells with a computed θ near unity. It seems reasonable to infer that the process of capture in N_2 and Ar is

[22] I. S. Dimitriev and V. S. Nikolaev, Zh. Eksperim. i Teor. Fiz. 44, 660 (1963) [English transl.: Soviet Phys.—JETP 17, 447 (1963)].

[23] D. R. Bates in *Atomic and Molecular Processes*, edited by D. R. Bates (Academic Press Inc., New York, 1962), p. 585.

[24] See Ref. 23, p. 595.

TABLE VI. Estimate of the cross section for capture of one electron by a C^{6+} ion with $\varepsilon=3$ MeV/amu in hydrogen, nitrogen, and argon.[a]

Gas	Shell	$Z-k$	a_p/a_0	I_p (keV)	$\frac{1}{2}mv^2-I_q+I_p$ (keV)	$(c_p/a_0)^2$	a_{pq}/a_0	θ	$(c_p/a_0)^2\theta$	$\sigma/\pi a_0^2$
H_2	K	1	1	0.013	1.18	0.0640	1.64	1.96×10^{-4}	1.2×10^{-5}	1.2×10^{-5}
N_2	K	7	0.143	0.666	1.82	0.0270	0.120	7.65×10^{-1}	2.1×10^{-2}	
				0.551	1.71	0.0305				
	L	5	0.800	0.098	1.26	0.0562	1.17	5.42×10^{-3}	3.0×10^{-4}	
				0.014	1.17	0.0652		6.28×10^{-3}	4.1×10^{-4}	4.1×10^{-2}
Ar	K	18	0.0546	4.42	5.58	0.0029	0.194	2.06×10^{-1}	6.0×10^{-4}	
	L	15	0.267	0.87	2.03	0.0216	0.225	7.79×10^{-1}	1.7×10^{-2}	
				0.42	1.58	0.0356		1.30	3.6×10^{-2}	
	M	8	1.125	0.143	1.30	0.0527	1.95	7.36×10^{-3}	3.9×10^{-4}	
				0.015	1.17	0.0650		1.14×10^{-2}	7.4×10^{-4}	2.3×10^{-1}

[a] For the carbon ion $a_q/a_0=0.166$ and $I_q=0.49$ keV. The kinetic energy of an electron with $\varepsilon=3$ MeV/amu is 1.65 keV.

qualitatively different than in H_2, and that in N_2 most of the cross section is due to the two K electrons, while in Ar it is mostly due to the eight L electrons.

Similar interpretation has been made of measurements of the capture cross sections of heavy ions with energies of 0.04 to 0.8 MeV/amu. To demonstrate that there is preferential capture of electrons with orbital velocity close to the ion velocity, the cross section, averaged over several ions at ion velocities equal to those of the electrons in the outermost and next-to-outermost shells of the atom, is shown to be roughly proportional to the number of electrons in those shells.[25]

If computations similar to those shown in Table VI are carried out for the conditions of Table I, a value for σ_{65} of $4\times10^{-7}\pi a_0^2$ is obtained. Because the value of σ_{65}/σ_{56} determined from Fig. 3 is about twice as large as that shown in the more accurate results of Fig. 4, the experimental capture cross section can be set equal to $1\times10^{-6}\pi a_0^2$, in closer agreement with the above estimate.

C. Interpretation of Results in Gases

Table VII shows the estimated values of the cross sections and the estimated and measured population ratios. Even though the estimated cross sections change by several orders of magnitude in the various stopping materials, the variation of the population ratio is qualitatively reproduced. The anomalously large values of ϕ_6/ϕ_5 in hydrogen reflect the extremely small value of σ_{65} in this case, attributed to the absence of a shell from which capture is highly probable.

D. The Increased Charge in Solids

The higher charge of carbon ions in solids than in gases at 3 MeV/amu may be interpreted in terms of the residual excitation of the ion as it enters a charge-changing collision.[26] The excitation of an electron initially captured in an excited state is determined by the ratio τ/τ_r, where τ is the time between charge-changing collisions and τ_r is the time required for an excited electron to return to the ground state. If $\tau<\tau_r$ the electron will on the average still be in an excited state when the ion undergoes a charge-changing collision; the loss cross section will be larger, and the average charge of the ion higher.

The times may be computed and the behavior of the ion examined with regard to τ/τ_r. The radiation time can be estimated from the probability of spontaneous emission, which is[27]

$$1/\tau_r\approx 4e^2\omega^3a_0^2/3\hbar c^3. \quad (14)$$

The value for τ_r shown in Table VIII is computed using

TABLE VII. Comparison of estimated and measured population ratios for carbon ions at 3 and 9 MeV/amu.

ε	Gas	$\sigma_{56}/\pi a_0^2$	$\sigma_{65}/\pi a_0^2$	σ_{56}/σ_{65}	ϕ_6/ϕ_5
3	H_2	1.68×10^{-3}	1.25×10^{-5}	1.4×10^{2}	28
3	N_2	4.70×10^{-2}	4.17×10^{-2}	1.1	2.2
3	Ar	0.287	0.229	1.3	1.7
9	H_2	6.00×10^{-4}	1.74×10^{-7}	3.5×10^{3}	900
9	N_2	1.68×10^{-2}	1.96×10^{-3}	8.6	90
9	Ar	0.102	1.47×10^{-2}	6.9	49

TABLE VIII. Estimates of the time τ_r for radiation of excitation energy and the time τ between collisions for a carbon ion with $\varepsilon=3$ MeV/amu.

τ_r (sec)	1.2×10^{-14}			
$\sigma_{56}/\pi a_0^2$	0.05	0.05	0.001	0.001
State	Gas	Solid	Gas	Solid
A/ρ (cm^3)	10^4	10	10^4	10
τ (sec)	1.6×10^{-12}	1.6×10^{-15}	7.9×10^{-11}	7.9×10^{-14}
Result	Diffuse	Dense	Diffuse	Diffuse

[25] V. S. Nikolaev, I. S. Dimitriev, L. N. Fateeva, and Ya. A. Teplova, Zh. Eksperim. i Teor. Fiz. **40**, 989 (1961) [English transl.: Soviet Phys.—JETP **13**, 695 (1961)].

[26] N. Bohr and J. Lindhard, Kgl. Danske Videnskab. Selskab, Mat. Fys. Medd. **28**, No. 7 (1954).

[27] See, for example, W. Heitler, *The Quantum Theory of Radiation* (Oxford University Press, Oxford, England, 1954), p. 178.

$\hbar\omega$ equal to the difference between the 5th and 6th ionization potentials of the carbon atom. The time between collisions is given by

$$\tau = A/(N_0 v \rho \sigma_{56}), \tag{15}$$

where A is the atomic weight and ρ the density of the stopping substance, N_0 is Avogadro's number, and σ_{56} the loss cross section. In Table VIII, v has been taken to correspond to $\mathcal{E}=3$ MeV/amu, and two illustrative values are taken for σ_{56}.

The value of τ is seen to be much longer than τ_r in gases; the gases are "diffuse" in the sense that the distance between charge-changing collisions is long enough so that an ion enters a collision in its ground state. In solids, however, the time between collisions is much shorter, and if the loss cross section is large enough the solid becomes "dense."

The variation of the charge between solids and gases shown in Fig. 8 may be interpreted in terms of the value of the loss cross section. If σ_{56} in Zapon and aluminum is of the same order of magnitude as that shown for nitrogen and argon in Table VII, these solids will be dense at $\mathcal{E}=3$ MeV/amu and the carbon ion will have a higher charge than it has in the gases. At $\mathcal{E}=8$ MeV/amu, σ_{56} may be expected to decrease, so that the solids will become diffuse and the charge will be the same in solids and gases. The value of σ_{56} at $\mathcal{E}=9$ MeV/amu shown for nitrogen in Table VII is sufficiently small to ensure that a solid with the same cross section would be diffuse, while the value for argon is probably much smaller than the one shown, because of the overestimate of the free collision approximation in high Z materials. The decrease in the difference between the charge in solids and gases as the velocity of the ion increases may thus be ascribed to a decreasing loss cross section.

VII. CONCLUSION

The equilibrium fractions of carbon ions with $+6$, $+5$, and $+4$ electronic charges have been measured as a function of the energy of the ions in hydrogen, nitrogen, and argon gases and in the solid nickel. Magnetic deflection was used to separate the ions of different charge states and a single junction counter used to register the number of ions in all states. The spatial separation of ions of different charge was converted into an energy separation, detectable by the counter, through the use of suitable aluminum foils. Estimated accuracies of about ± 0.05 MeV/amu in the energy and as low as ± 0.002 in the equilibrium fractions were obtained.

The equilibrium populations were found to be slightly different functions of energy for the different stopping substances. The rms charge calculated from the populations at 3 MeV/amu is higher in solids than gases, if hydrogen gas is excepted, but is the same in solids and gases at 8 MeV/amu. In hydrogen the rms charge is anomalously high at all energies.

In order to interpret the charge in hydrogen, a rough method for calculating the electron capture and loss cross sections of C^{6+} and C^{5+} ions is given. The loss cross sections are estimated in the Bohr free collision approximation, and the capture cross sections in the Born approximation. In nitrogen and argon capture proceeds from the K and L shells, respectively, and the anomaly in hydrogen is apparently due to the lack of a similar shell from which capture is highly probable.

The increased charge at low energies in solids is consistent with a loss cross section increased by residual excitation of the ion. In gases, the time between collisions is much longer than the time for radiation, and no residual excitation is expected. At high energies in solids, the decrease in loss cross section with energy results in a long enough time between collisions for the ion to lose its excitation.

ACKNOWLEDGMENTS

The advice of Dr. L. C. Northcliffe was instrumental during the early stages of experimentation, and he kindly read portions of this article. Kenneth Klotz and Jonathan Rodnick, Bursary Students in Yale College, plotted nearly 300 100-channel analyzer spectra and performed many of the computations.

The efforts and cooperation of the operating staff of the Heavy Ion Accelerator, under the direction of Professor R. Beringer, are gratefully acknowledged.